



Microscopic foundation of the $\mu(I)$ rheology for dense granular flows on inclined planes

Denis Dumont, Haggai Bonneau, Thomas Salez, Elie Raphael, Pascal Damman

► To cite this version:

Denis Dumont, Haggai Bonneau, Thomas Salez, Elie Raphael, Pascal Damman. Microscopic foundation of the $\mu(I)$ rheology for dense granular flows on inclined planes. 2022. hal-03696161v1

HAL Id: hal-03696161

<https://hal.science/hal-03696161v1>

Preprint submitted on 23 Jun 2022 (v1), last revised 30 Sep 2022 (v2)

HAL is a multi-disciplinary open access archive for the deposit and dissemination of scientific research documents, whether they are published or not. The documents may come from teaching and research institutions in France or abroad, or from public or private research centers.

L'archive ouverte pluridisciplinaire **HAL**, est destinée au dépôt et à la diffusion de documents scientifiques de niveau recherche, publiés ou non, émanant des établissements d'enseignement et de recherche français ou étrangers, des laboratoires publics ou privés.

Microscopic foundation of the $\mu(I)$ rheology for dense granular flows on inclined planes

Denis Dumont,¹ Haggai Bonneau,² Thomas Salez,³ Elie Raphael,² and Pascal Damman^{1,*}

¹*Laboratoire Interfaces & Fluides Complexes, Université de Mons, 20 Place du Parc, B-7000 Mons, Belgium.*

²*UMR CNRS Gulliver 7083, ESPCI Paris, PSL Research University, 75005 Paris, France.*

³*Univ. Bordeaux, CNRS, LOMA, UMR 5798, F-33400 Talence, France.*

(Dated: June 15, 2022)

Macroscopic and microscopic properties of dense granular layers flowing down inclined planes are obtained from Discrete-Element-Method simulations for both frictionless and frictional grains. Linear dilatancy laws with the inertial number I are observed. They do not depend on the frictional nature of the grains besides the value of the jamming packing fraction. In sharp contrast, for the friction law relating the effective, macroscopic friction coefficient μ to the inertial number, two distinct behaviors are observed: a linear relationship with I for frictional grains and a square root evolution for frictionless ones. Regarding the microscopic properties of the flowing grains, a temperature is defined from the velocity fluctuations, and related to the diffusion coefficient along the direction perpendicular to the flow. A correlation length emerges from the dimensionless fluctuations. The microscopic description of the granular system allows us to propose a theoretical foundation for the macroscopic laws and to recover the Bagnold velocity profile and the $\mu(I)$ rheology observed for frictionless systems.

Despite several decades of intense research, the mechanisms underlying dense granular flows remain largely misunderstood. A universal framework allowing one to describe the numerous configurations and observations studied in the laboratory is still lacking [1]. Most models remain semi-empirical and are not supported by strong microscopic justifications [2–7]. The global flow properties are usually described from the popular $\mu(I)$ rheology. This approach consists in two empirical relations between the macroscopic friction coefficient μ (defined as the ratio between the shear stress and the pressure) or the volume fraction ϕ on one hand, and the inertial number $I = \dot{\gamma}d\sqrt{\rho_p/P}$ on the other hand, involving the shear rate $\dot{\gamma}$, the grain size d , the mass density $\rho_p \sim m/d^3$ of the grains, their individual mass m , and the pressure P [2, 8]. Essentially, in this Amontons-Coulomb-like description, a granular layer starts to flow when the applied shear stress overcomes a critical frictional stress $\mu_c P$. Nevertheless, this description fails to properly rationalize some important observable features, such as the presence of a metastable region [9, 10] and the layer-thickness dependence of the angle at which the flow stops [11–14].

In this Letter, using a combination of Discrete-Element-Method (DEM) simulations and a model based on microscopic arguments, we address the rheology of dense granular matter from the canonical setting of a layer flowing down an inclined plane. Therein, the inclination angle θ and the layer thickness H are the two external control parameters. Previous experimental and numerical studies have shown that the local average velocity profile of a thick granular layer flowing over an inclined plane exhibits a so-called Bagnold profile [1, 15, 16], *i.e.* $\langle v(z, t) - v(0, t) \rangle \sim H^{3/2} - (H - z)^{3/2}$, where $v(z, t)$ is the local velocity field along the flow direction, at normal coordinate z and time t . As a remark, we have the relation $\dot{\gamma}(z) = d\langle v(z, t) \rangle/dz$. The averages

$\langle \rangle$ are performed over time and realizations, at fixed z . Besides, it has been suggested that nonlocal cooperative effects are essential to describe the layer-thickness dependence of the stop angle [17, 18], *i.e.* the smallest angle for which a stationary flow is observed. We will see here that cooperative effects are also of prime importance in order to understand the velocity profiles of dense granular flows, as well as the two empirical relations, $\mu(I)$ and $\phi(I)$, commonly used to fit experimental and numerical data [2, 8].

The numerical simulations were performed with the software LIGGGHTS [19]. The system consists in a layer of identical grains, with diameter $d = 1$ mm and mass $m = \frac{4}{3}\pi\rho_p d^3$, placed on an inclined plane with an inclination angle θ (see Fig. 1a). We focus here on thick-enough layers, in order to avoid the thickness dependence of the stop angle observed for thin layers [11–14]. The mechanical properties of the simulated grains are set to be exactly the same as in our previous study [17], and correspond to glass beads [11]. In particular, the microscopic coefficients μ_s and μ_r of sliding and rolling frictions are set to 0.5 and 0.01 (different friction coefficients have also been studied, see SI [20]), respectively. In addition, frictionless grains (*i.e.*, $\mu_s = \mu_r = 0$) are also simulated. The substrate is made of immobile grains to mimic the glued grains in inclined-plane experiments. We impose periodic boundary conditions in the x and y directions to get rid of side-wall effects [21]. The size of the base has been carefully chosen in order to be large enough to avoid autocorrelations due to periodicity. We stress that similar setups have already been reported [9, 15, 16].

Before inclination of the plane, the layer has an initial vertical thickness H_i ranging between $10d$ and $60d$, with a base of $20d \times 20d$ in the horizontal plane. The plane is subsequently inclined briefly at 30° to initiate the flow. Subsequently, the inclination is fixed at the desired angle

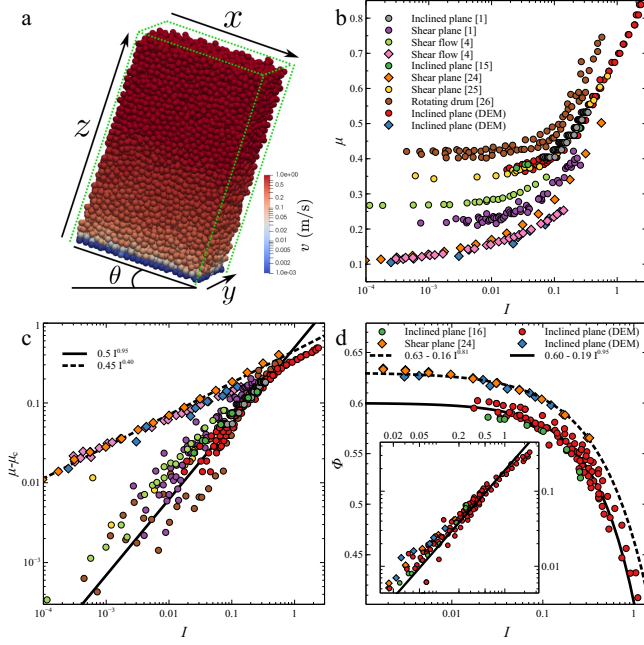


FIG. 1. a) Typical snapshot of a DEM simulation, with initial layer thickness $H_i = 30d$ and inclination angle $\theta = 24^\circ$. The color code indicates the velocity $v(z, t)$. b) Macroscopic friction coefficient μ as a function of inertial number $I = \dot{\gamma}d\sqrt{\rho_p/P}$ for frictionless (diamonds) and frictional (circles) grains, as well as various inclination angles θ , initial layer thicknesses H_i , and various setup configurations [1, 4, 16, 24–26]. c) Difference $\mu - \mu_c$ in friction coefficient as a function of inertial number I , where $\mu_c = \mu(I \rightarrow 0)$, for the same data as in the previous panel. The solid and dashed lines indicate fitted expressions, as provided in legend. d) Volume fraction ϕ as a function of inertial number I for frictionless (diamonds) and frictional (circles) grains. Data from [16, 24] are added for comparison. The solid and dashed lines indicate fitted expressions, as provided in legend. The inset shows the difference $\phi_c - \phi$ in volume fraction as a function of I , where $\phi_c = \phi(I \rightarrow 0)$, for the same data. The solid line corresponds to $\phi_c - \phi = 0.19I$.

θ , ranging between 20° and 40° . For each value of H_i and θ , the actual layer thickness H along z , and the mean volume fraction ϕ of the whole layer (averaged over at least 10 time steps in the steady state) are measured. The average local velocity profiles $\langle v(z, t) \rangle$ and the inertial number I are also computed.

In agreement with previous works [1, 9, 15, 16], we observe that: i) there is a critical stress to induce flow for dense granular layers, corresponding to a macroscopic friction coefficient $\mu_c \approx 0.35$ for frictional grains, and 0.1 for frictionless grains (Fig. 1b); ii) the local average velocity profile is well described by a Bagnold profile (see Fig. S2a in SI [20]); iii) the volume fraction ϕ (see Fig. S2b in [20]) and the inertial number I (see Fig. S2c in SI [20]) remain mostly constant throughout the layer, for all the studied inclination angles. As proposed in sev-

eral studies [8, 22, 23], dimensional analysis shows that only a single dimensionless parameter is required to describe granular flows, *i.e.*, the inertial number I (besides the microscopic friction coefficient). The flow properties are characterized through the frictional, $\mu = \mu(I)$, and the dilatancy, $\phi = \phi(I)$ laws. The macroscopic friction coefficient μ is determined by the shear to normal stress ratio [2, 8, 23]. For the inclined-plane geometry considered here, both the macroscopic friction coefficient and the pressure are prescribed through the inclination θ of the plane and the height H of the flowing layer [23]. In a continuum-limit approximation, the effective friction coefficient for this setup is thus fixed to a constant value, $\mu = \tan(\theta) \simeq \theta$ for the range of inclination angles of interest. From dimensional analysis and since μ does not depend on z/d , we can conclude that I and ϕ are constant throughout the layer and fully determined by the incline angle θ and the microscopic friction coefficient.

As previously shown, and up to moderate incline angles ($I \lesssim 0.1$), Fig. 1c confirms that $\mu(I)$ is well described by $\mu - \mu_c \sim I^\alpha$, with $\alpha \approx 0.4$ – 0.5 for frictionless grains [4, 24], and $\alpha \approx 1$ for frictional ones [1, 16, 25, 26]. The latter exponent does not depend on the (finite) values of the microscopic friction coefficients (see Fig. S1a in [20]), thus indicating the singularity of the frictionless limit. In contrast, μ_c does depend on the microscopic friction coefficients, but even for frictionless assemblies a non-zero value close to 0.1 is observed [14, 20, 24]. The exact origin of this residual macroscopic friction remains unclear, but should be related to the steric constraints associated with granular topography [27].

The dilatancy laws obtained from the DEM simulations are shown in Fig. 1d and compared to data from the literature. Despite other functional forms were proposed [24], the evolution of the packing fraction with I can be empirically described by the simple relation $\phi_c - \phi \sim I^\beta$, where $\phi_c = \phi(I \rightarrow 0)$ is the volume fraction at kinetic arrest, and with $\beta \approx 0.8$ – 1 , for both the frictionless and frictional cases.

Hereafter, we investigate the microscopic origin of these laws. As proposed by several authors, the velocity fluctuations and the diffusion coefficient of the grains are strong indicators of their dynamics [28, 29]. A dense granular flow is characterized by rapid collisions involving sudden changes of the velocity direction and renewal of the contact network. Assuming that all these events occur at high frequency compared to the evolution of mean-field quantities, they can be described through a granular temperature [22]. A reasonable assumption is to consider that this temperature is related to the local velocity fluctuations, through the proportionality relation $k_B T(z) \sim m \delta v^2(z)$, with $\delta v^2(z) = \langle |v(z, t) - \langle v(z, t) \rangle|^2 \rangle$ the local variance of the velocity field $v(z, t)$ along the flow direction. Figure 2b shows the evolution of the dimensionless standard deviation $\overline{\delta v}/(d\sqrt{\gamma})$, where $\overline{A} = \frac{1}{H} \int_0^H dz A(z)$ represents the thickness average of $A(z)$, as a function of

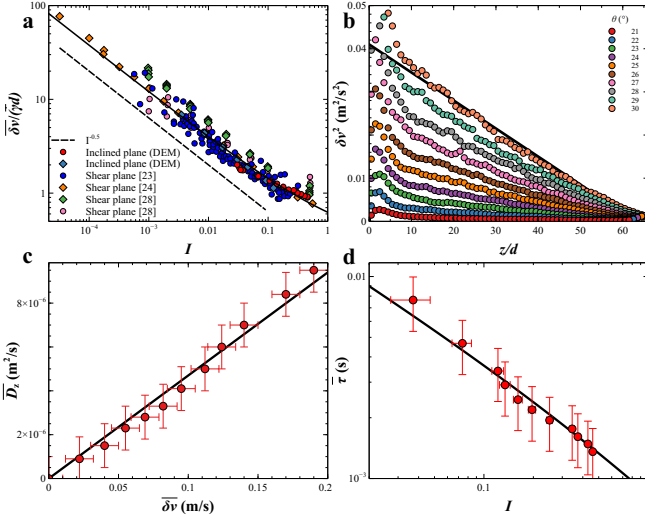


FIG. 2. a) Thickness-averaged standard deviation $\overline{\delta v}$ of the velocity field normalized by a typical shear velocity $\bar{\gamma}d$, as a function of the inertial number I , for frictionless (diamonds) and frictional (circles) grains. Results from previous works [23, 24, 28] are also shown for comparison. The dashed line indicates a $\sim I^{-1/2}$ power law as a guide to the eye. The solid line corresponds to $a(1 + b/\sqrt{I})$ with $a=0.25$ and $b=1.5$. b) Local variance $\delta v^2(z) = \langle |v(z, t) - \langle v(z, t) \rangle|^2 \rangle$ of the velocity field $v(z, t)$, as a function of rescaled normal coordinate z/d , for a layer of frictional grains initially characterized by $H_i = 60d$ and various inclination angles θ as indicated. An affine solid line is added as a guide for the eye. c) Thickness-averaged diffusion coefficient \overline{D}_z along z as a function of the thickness-averaged standard deviation $\overline{\delta v}$ of the velocity field for frictional grains. The solid line corresponds to a linear fit. d) Correlation time $\bar{\tau}$ of the thickness-averaged velocity fluctuations (see Fig. S3b in SI [20]) as a function the inertial number I . The black solid line corresponds to $0.26 d/(l_c \bar{\gamma})$, with $l_c/d = a(1 + b/\sqrt{I})$ with $a=0.25$ and $b=1.5$ found in panel a.

the inertial number, for frictional and frictionless grains. We stress that the dimensionless standard deviation is independent of z due to the Bagnold profile satisfied by $\langle v(z, t) \rangle$ (see Fig. S2a in SI [20]) and the affine spatial behaviour of the variance observed in Fig. 2a. Interestingly, no matter the frictional nature of the grains, all the data reported here and in the literature collapse onto a single master curve showing a decrease of the relative velocity fluctuations with increasing inertial number. For small I values, the dimensionless standard deviation decreases as $I^{-0.5}$, while it seems to saturate to a constant value at large I [28]. Interpolating the two asymptotic behaviours through a simple crossover form, one gets $\overline{\delta v}/(d\bar{\gamma}) = a(1 + b/\sqrt{I})$, that fits well the data.

Let us now investigate the impact of the effective thermal energy on the grain dynamics. As shown by the time evolution of their thickness-averaged mean-square displacement along z (see Fig. S3a in SI [20]), the grains

globally diffuse perpendicularly to the flow direction, at long time with an associated thickness-averaged diffusion coefficient \overline{D}_z increasing with the incline angle θ . Furthermore, as shown in Fig. 2c, \overline{D}_z increases linearly with the thickness-averaged standard deviation $\overline{\delta v}$ of the velocity field. This linear relation can be understood from the thickness-averaged Kubo relation:

$$\overline{D}_z = \int dt \langle w(z, t) w(z, 0) \rangle \sim \tau(z) \overline{\delta v^2(z)} \sim d \overline{\delta v}, \quad (1)$$

with $w(z, t)$ the velocity field along z , at position z and time t , and where we assumed isotropic local velocity correlations of amplitude $\delta v^2(z)$ decaying in an exponential fashion over a local characteristic time $\tau(z) \sim d/\delta v(z)$. In addition, given the affine trends in Fig. 2b, one can show that $\bar{\tau} \sim d/\overline{\delta v}$. The thickness-averaged temporal correlations functions $\langle w(z, t) w(z, 0) \rangle$ of the velocity field along z , as calculated from the DEM trajectories (see Fig. S3b in SI [20]), appear to decay faster with increasing θ . Given the affine trends in Fig. 2b, and neglecting long-time power-law tails, we can show that the exponential-decay time of $\langle w(z, t) w(z, 0) \rangle$ is well approximated by $\sim \bar{\tau}$. Besides, the velocity correlations suggest the existence of dynamic clusters that persist over the correlation time. We thus hypothesize the existence of a characteristic, mesoscopic and *a priori* z -dependent size $l_c(z)$ over which dynamic clusters persist during the time $\tau(z)$. This is reminiscent of the vortices discussed by Kharel and Rognon [28]. As proposed by DeGiuli *et al.*, these clusters produce an amplification of the velocity fluctuations that is estimated through a “lever” effect [30]. Specifically, one has $l_c(z) \sim d/[\tau(z)\dot{\gamma}(z)]$, and, with the definition $\tau \sim d/\delta v$, one gets $\delta v(z)/[d\dot{\gamma}(z)] \sim l_c(z)/d$ where the amplification factor appears clearly. Interestingly, since the left-hand side of the latter relation is independent of z , as discussed above, one gets that the dynamic-cluster size l_c is in fact independent of z for the inclined-plane configuration. Finally, invoking the crossover relation between the two asymptotic regimes of $\overline{\delta v}/(d\bar{\gamma})$, one gets $l_c/d \sim 1 + 1.5/\sqrt{I}$. For small I values, one has $l_c \sim d/\sqrt{I}$, while for large I , $l_c \sim d$. Figure 2d shows $\bar{\tau}$, as estimated from the thickness-averaged temporal correlations functions (see Fig. S3b in SI [20]), as a function of I . The data is in agreement with the relation derived from l_c above. Since the latter is based on the crossover expression between the two asymptotic regimes of Fig. 2a, which is independent of the frictional nature of the grains, this agreement suggests that the size of the dynamic clusters is mainly determined by the collisions between grains, but not by the microscopic friction between them. Furthermore, from Fig. 2a this dynamic-cluster size is expected to diverge at kinetic arrest – which is reminiscent of the hypothetical cooperative length associated with the glass and jamming transitions. It should however be noted that some influence of the microscopic friction coefficient has been observed by DeGiuli and Wyart [30],

but for very small I values that are well below the range accessed here.

In the following, we aim deriving the macroscopic rheological laws from the microscopic fluctuations and correlations. From dimensional analysis, we have recalled that a single parameter determines the flow properties. In the inclined-plane geometry, all dimensionless parameters are uniquely determined by the incline angle $\theta \simeq \mu$. Therefore, the dimensionless ratio $Pd^3/(k_B T)$ should be constant in the layer for inclined-plane experiments. In a continuous mean-field approximation, the pressure field is hydrostatic, *i.e.* $P(z) = \phi \rho_p g(H - z)$. It thus follows that the effective temperature must vary with the depth according to $T(z) \propto (H - z)$. As observed in Fig. 2b, apart from slight boundary deviations, the affine relation $\delta v^2(z) \propto (H - z)$ is satisfied for all the tested inclination angles θ , which supports the definition of the effective temperature through $k_B T(z) \sim m \delta v^2(z)$. Interestingly, the effective temperature and the associated mechanical noise are maximal near the substrate and vanish at the free interface. This suggests that the collisions between mobile grains and the glued ones at the substrate is the source of temperature in the system. Furthermore, using the definition of the inertial number, the pressure can be written as $P(z) \sim m \dot{\gamma}(z)^2 / (d I^2)$. Combining this relation with $\delta v(z) \sim l_c \dot{\gamma}(z)$, and the definition of the effective temperature, one gets $Pd^3/(k_B T) \sim d^2/(l_c^2 I^2)$. For small inertial numbers, $l_c \sim d I^{-1/2}$, and thus $Pd^3/(k_B T) \sim 1/I$. By identifying the latter relation to the equation of state (EOS) for hard-sphere fluids near the jamming transition [31, 32], *i.e.* $Pd^3/(k_B T) = \phi_J/(\phi_J - \phi)$, one gets the dilatancy law:

$$\phi_J - \phi \sim I. \quad (2)$$

As shown in Fig. 1d, this law agrees with all the data from our DEM simulation and the literature, for small inertial numbers, provided that ϕ_J is replaced by ϕ_c . The universal agreement for both frictionless and frictional grains can be related to the evolution of the cluster size with inertial number, and reflects once again the dominance of collisions over friction in the dynamics. The validity of the hard-sphere-fluid EOS is probably limited to the intermediate range of inertial numbers, *i.e.* $0.01 \lesssim I \lesssim 0.5$, where the granular system can be considered as a fluid and where the mechanical noise ensures that no long-range correlations develop. For $I \lesssim 10^{-3}$, the system should behave as an amorphous layer, and deviations from the current dilatancy law might appear.

Let us finally propose a microscopic picture for the $\mu(I)$ rheological law. To do so, we consider the steady-state balance of driving and dissipated powers for a test grain located in a slab of thickness d at height z . First, to estimate the driving contribution, we consider that the grain experiences the sum of gravitational and friction forces projected in the flow direction, and that θ

and θ_c are small, leading to an effective driving force $\sim \rho_p \phi g(H - z) d^2 (\theta - \theta_c)$. Since the grain moves over a distance d within a time $\dot{\gamma}(z)^{-1}$, the net local driving power is $\dot{W}_d(z) \sim \rho_p \phi g(H - z) d^3 (\theta - \theta_c) \dot{\gamma}(z)$. Secondly, we assume that the energy is mainly dissipated through the collisions with other grains, characterized by the characteristic decay time $\tau(z) \sim d/[l_c \dot{\gamma}(z)]$. The local power dissipated by collisions can thus be estimated by $\dot{W}_c(z) \sim m \delta v^2(z)/\tau(z)$. Balancing $\dot{W}_d(z)$ with $\dot{W}_c(z)$, and recalling that $\delta v \sim \dot{\gamma} l_c$ leads to $\dot{\gamma}^2 \sim g d \phi (H - z) (\theta - \theta_c)/l_c^3$. At small angles, and thus small I , Fig. 2a shows that $l_c \sim d I^{-1/2}$. Inserting this expression in the previous one, together with the definition of I , yields the general relation:

$$\dot{\gamma} \sim \left[\frac{g \phi (H - z)}{d^2} \right]^{1/2} (\theta - \theta_c)^2. \quad (3)$$

First, this expression is compatible with the z -dependency of the Bagnold velocity profile, $\langle v(z, t) - v(0, t) \rangle \propto H^{3/2} - (H - z)^{3/2}$. Secondly, recalling that $\mu \simeq \theta$, as well as the definition of I , Eq. (3) yields the friction law $\mu - \mu_c \sim I^{0.5}$, that is very close to the law observed for frictionless grains in Fig. 1c.

One may naively expect Eq. (3) to also hold for frictional systems, since the velocity fluctuations and cluster size behave similarly with the inertial number for both frictional and frictionless systems. However, it can not explain the $\mu - \mu_c \sim I$ relation observed for frictional grains in Fig. 1c. This disagreement is in fact not surprising. In the derivation of Eq. (3), it is assumed that all the energy dissipation arises from collisions between grains. This is a very reasonable assumption for frictionless systems, but an additional source of dissipation is expected from the mobilization of frictional contacts. Unfortunately, including frictional dissipation in a theoretical model for dense granular flows remains a highly debated issue [25, 30]. Nevertheless, interestingly, Fig. 1c shows that for large-enough inertial numbers, the data obtained for frictional systems collapse onto the law of frictionless systems. This observation suggests that, in the limit of large I , the energy dissipation is universal and of collisional origin.

In summary, from numerical simulations and inspection of the literature data, we show that the dilatancy law is identical for frictionless and frictional assemblies. This law can be further rationalized from a comparison between: i) the equation of state constructed from the hydrostatic pressure, an effective granular temperature related to velocity fluctuations, as well as the inertial number; and ii) the equation of state of hard-sphere fluids near the jamming transition. In contrast, the macroscopic friction laws are observed to differ for frictionless and frictional assemblies. In the former case, we can rationalize the observations from a power balance at the grain level, involving gravity, effective friction, and collisions. We recover as well the Bagnold profile for the

local average velocity field. The derivation of a macroscopic friction law for frictional assemblies remains an open question and should involve an additional dissipation term related to the formation of frictional contacts.

The authors thank Yoel Forterre, Olivier Pouliquen, Olivier Dauchot and Pierre Soulard, for enlightening suggestions. This work benefited from financial support of the Fonds National de la Recherche Scientifique through the PDR research project T.0251.20 “Active matter in harmonic traps”, the Foundation for Training in Industrial and Agricultural Research, the Agence Nationale de la Recherche (ANR-21-ERCC-0010-01 *EMet-Brown*, ANR-21-CE06-0029 *SOFTER*, ANR-21-CE06-0039 *FRICOLAS*), and the French Friends of the Hebrew University of Jerusalem and the Scopus Foundation. The authors also thank the Soft Matter Collaborative Research Unit, Frontier Research Center for Advanced Material and Life Science, Faculty of Advanced Life Science at Hokkaido University, Sapporo, Japan.

* pascal.damman@umons.ac.be

- [1] MiDi, GDR. *The European Physical Journal E* **14**, 341–365 (2004)
- [2] Jop, P., Forterre, Y. & Pouliquen, O. *Nature* **441**, 727–730 (2006).
- [3] Bouchaud, J.-P., Cates M.E., Ravi Prakash, J., & Edwards, S.F. *J. Phys. I France* 1383–1410 (1994).
- [4] Bouzid, M., Trulsson, M., Claudin, P., Clément, E. & Andreotti, B. *Phys. Rev. Lett.* **111**, 238301 (2013).
- [5] Bouzid, M., Izzet, A., Trulsson, M., Clément, E., Claudin, P. & Andreotti, B. *Eur. Phys. J. E* **38**, 125 (2015).
- [6] Kamrin, K. & Koval G. *Phys. Rev. Lett.* **108** 178301 (2012).
- [7] Kamrin, K. *Frontiers in Physics* **7**, 116 (2019).
- [8] Andreotti, B., Forterre, Y. & Pouliquen, O. Cambridge University Press, 2013.
- [9] Silbert, L.E., Landry, J.W., & Grest, G.S. *Physics of Fluids* **15**, 1-10 (2003).
- [10] Forterre, Y. & Pouliquen, O. *Journal of Fluid Mechanics* **486**, 21-50 (2003).
- [11] Pouliquen, O. *Phys. Fluids* **11**, 542–548 (1999).
- [12] Borzsonyi, T., Halsey, T.C. & Ecke, R.E. *Phys. Rev. E* **78**, 011306 (2008).
- [13] Malloggi, F., Andreotti, B. & Clément, E. *Phys. Rev. E* **91**, 052202 (2015).
- [14] Perrin, H., Wyart, M., Metzger, B. & Forterre, Y. *Phys. Rev. Lett.* **126**, 228002 (2021).
- [15] Silbert, L.E., Ertas, D., Grest, G.S., Halsey, T.C., Levine, D. & Plimpton, S.J. *Phys. Rev. E* **64**, 051302 (2001).
- [16] Baran, O., Ertas, D., Halsey, T.C., Grest, G.S. & Lechman, J.B. *Phys. Rev. E* **74**, 051302 (2006).
- [17] Dumont, D., Soulard, P., Salez, T., Raphael, E. & Damman, P. *Phys. Rev. Lett.* **125**, 208002 (2020).
- [18] Kamrin, K. & Henann, D.L. *Soft Matter* **11**, 179–185 (2015).
- [19] C. Kloss, C. Goniva, A. Hager, S. Amberger, & S. Pirker. *Prog. Comput. Fluid Dyn.* **12**, 140-152 (2012).
- [20] See Supplementary Material at <http://link.aps.org/supplemental/>
- [21] Jop, P., Forterre, Y. & Pouliquen, O. *J. Fluid Mech.* **541**, 167-192 (2005).
- [22] Lois, G., Lemaître, A. & Carlson J.M. *Physical Rev. E* **72**, 051303 (2005).
- [23] Da Cruz, F., Emam, S., Prochnow, M., Roux, J.N. & Chevoir, F. *Physical Rev. E* **72**, 021309 (2005).
- [24] Peyneau, P.E. & Roux, J.N. *Phys. Rev. E* **78**, 011307 (2008).
- [25] Azema, E. & Radjaï, F. *Phys. Rev. Lett.* **112**, 078001 (2014).
- [26] Li, L. & Andrade, J.E. *Granular Matter* **22**, 52 (2020).
- [27] Peyneau, P.E. & Roux, J.N. *Phys. Rev. E* **78**, 041307 (2008).
- [28] Kharel, P. & Rognon, P. *Phys. Rev. Lett.* **119**, 178001 (2017).
- [29] Saitoh, K. & Kawasaki, T. *Frontiers in Physics* **8**, 99 (2020).
- [30] DeGiuli, E., McElwaine, J.N. & Wyart, M. *Phys. Rev. E* **94**, 012904 (2016).
- [31] Torquato, S. & Stillinger, F. *Rev. Mod. Phys.* **82**, 155501 (2007).
- [32] Parisi, G. & Zamponi, F. *Rev. Mod. Phys.* **82**, 789 (2010).